On Instantanous Behaviour of Microplastic Contaminants in Turbulent Flow

Arefeh Shamskhany and Shooka Karimpour

Abstract The global plastic waste generation increased drastically during the past decade, and therefore, microplastic (MP) input to the aquatic environment is growing exponentially. MP distribution in the aquatic environment is linked to particles' physical characteristics. However, due to different origins and exposure to various weathering processes, MPs possess an extensive range of densities, shapes, and sizes. Turbulent structure induced by different mechanisms, such as temperature gradient, wind, and sudden topography changes, is another dominant factor affecting MP transport and distribution. This study aims to investigate the combined effect of size and density on the entrainment and mixing behaviour of MPs in a turbulent flow induced over the backward facing step. We used well-known sediment analogy criteria to study MP mixing and entrainment. Settling parameter, Stokes number, and trapping radius are used in this study to understand the entrainment and distribution of MPs in turbulent structures with different turbulent intensities. The first parameter describes the particle entrainment in the ambient fluid, while the other two parameters describe the distribution and mixing behaviour of particles. Our analysis demonstrates universal trends for MPs entrainment and distribution with the ambient flow dominated by MP size and density, combined with the turbulent flow hydrodynamics.

Keywords Microplastic Contaminants in Turbulent Flow · Instantanous Behaviour

A. Shamskhany (✉) · S. Karimpour
Department of Civil Engineering, Lassonde School of Engineering, York University, Toronto, Canada
e-mail: shams019@yorku.ca

S. Karimpour
e-mail: shooka.karimpour@lassonde.yorku.ca

1 Introduction

Plastic generation has increased drastically over the last decade, leading to a proportional increase in plastic waste generation [14]. Mismanaged plastic wastes can get into aquatic environments through different pathways, such as rivers, wastewater treatment systems, and stormwater runoff. Plastic debris remains in the aquatic environment for countless years, where weathering processes break particles into smaller parts [3]. Therefore, the presence of microplastics (MPs), plastic particles sized smaller than 5 mm, will grow exponentially over the years. Despite their benefits, the exponential growth of plastics and the corresponding increase in MP abundance in aquatic environments resulted in critical environmental risks due to the detrimental impact on aquatics' health. The fragmentation process and diversity of origins result in a broad range of shapes and sizes for aquatic MPs, from infinitesimal spheres and fragments, which is difficult to detect with necked eye, to sheets and fibres in the size of small gravels. Also, MPs possess a miscellaneous range of polymers due to their origin and utilities [25, 27]. The physical characteristics of a particle are linked to its mobility and fate in the ambient flow. Therefore, the vast range of aquatic MPs' physical characteristics results in the unique behaviour of these particles. Recent studies demonstrate MPs' selective presence in different aquatic compartments, which is affected by particles' physical properties [6, 24]. Similar to sediment particles, MPs' motion is derived from the forces acting on them. The force balance between gravity, buoyancy, and drag of MP particles dictates the trajectory and fate of these particles. Therefore, many studies focus on the density and buoyancy of plastic polymers, which undeniably play key roles in MP distribution [9, 25]. However, MPs shape and size also affect the active force terms, especially drag, drag to buoyancy ratio, and therefore are undeniably important in particles' mobility and distribution [8, 18, 30]. Khatmullina and Isachenko [18] have conducted laboratory experiments to assess the settling patterns of regularly shaped sinking MPs in analogy with sediments. Wang et al. [31] also carried out laboratory settling experiments for irregularly shaped heavy MPs.

The absence of MPs from the surface layer can be associated with many factors, including biofouling, settling, and vertical mixing with the turbulent flow [19, 22, 17]. Turbulent diffusion plays a significant role in the vertical distribution and transport of MP particles [15, 13, 23]. Yet, hydrodynamics of MPs and the role of turbulent mixing on their distribution and transport has not been thoroughly studied. On the other hand, the wide range of physical properties makes the investigation of MPs' distribution and fate very complicated in the aquatic environment. However, the existing literature on sediments' mixing and entrainment can help understand the behaviour of MPs in turbulent aquatic systems [13, 18, 31]. The growing sediment analogy knowledge demonstrates the significant effect of size on particle mixing and entrainment with the turbulent flow [28, 11, 12]. Thus, MPs of varying sizes from 5 mm to 10 μm can have different trajectories and fates in the same flow. The aim of this paper is to study the entrainment and mixing behaviour of MP particles of various sizes and densities at different turbulent intensities. Here we conducted

numerical experiments in an open channel system using OpenFoam. Our numerical experiments include spherical MP particles ranging in size from $100\,\mu$m to 2 mm and densities associated with abundant polymers from buoyant polypropylene polyethylene to heavy polyethylene terephthalate particles. We injected these particles to fully developed two-dimensional turbulent flows of various intensities and observed their mixing and entrainment with the flow. Results of this study are quantified using dimensionless hydrodynamic parameters in sedimentology to explain the combined effect of size and density on MPs' entrainment with the turbulent flow.

2 Methodology

In the present study, simulations are conducted using OpenFOAM, an open-source computational fluidic tool. In using OpenFOAM, we modified one of the pre-existing hybrid Eulerian–Lagrangian solvers to adjust it to MPs' characteristics. MPs are injected into turbulent flows to investigate the effect of turbulent circulations on the vertical mixing and transport of particles. In order to induce a coherent turbulent structure, flow over a backward facing step (BFS) is modelled. Once the flow behind the step reaches a fully developed state, MP particles are injected into the turbulent ambient flow. This section provides an overview of governing equation and model setup for both Eulerian and Lagrangian particle-tracking sub-models.

2.1 Eulerian Sub-model

In the first step, the turbulent flow structure is simulated using the Eulerian sub-model. For this purpose, a set of conservation of mass and momentum equations are solved using a finite volume scheme:

$$\frac{\partial (\overline{u}_i)}{\partial x_i} = 0 \tag{1}$$

$$\frac{\partial \overline{u}_i}{\partial t} + \frac{\partial \left(\overline{u}_i \overline{u}_j\right)}{\partial x_j} = -\frac{1}{\rho_f}\frac{\partial \overline{p}}{\partial x_i} + \nu \frac{\partial^2 \overline{u}_i}{\partial x_j x_j} - \frac{1}{\rho_f}\frac{\partial \tau_{ij}^{\mathrm{SGS}}}{\partial x_i} \tag{2}$$

where ρ_f is the density of the ambient flow, which in our simulations, it is assumed as 1020 kg/m^3 (the density of seawater), $\overline{p}$ is the pressure, ν is the kinematic viscosity of the fluid, $\overline{u}_i$ is the velocity of the flow, and τ_{ij}^{SGS} represents turbulent stresses. The turbulent flow over the BFS is modelled using the large eddy simulation (LES) turbulent modelling approach. Grid size selection is critical in the LES model, as turbulent scales larger than the grid size are resolved, while the effect of smaller than scale, i.e. grid size, is modelled. In the present study, Smagorinsky sub-grid-scale viscosity is used [26]:

$$\tau_{ij}^{\text{SGS}} - \frac{1}{3}\tau_{kk}\delta_{ij} = 2\nu_t \overline{S}_{ij} \tag{3}$$

$$\nu_t = C_s\Delta^2\sqrt{2\overline{S}_{ij}\overline{S}_{ij}} \tag{4}$$

$$\overline{S}_{ij} = \frac{1}{2}\left(\frac{\partial \overline{u}_i}{\partial x_j} + \frac{\partial \overline{u}_j}{\partial x_i}\right) \tag{5}$$

where ν_t is the turbulent viscosity, S_{ij} is the strain rate tensor, δ_{ij} is the Kronecker delta tensor, $\Delta = \sqrt{dxdy} = dx$ is the grid size, and $C = 0.094$ is the Smagorinsky constant used in current simulations.

2.2 Lagrangian Sub-model

Ambient flow hydrodynamics affect the trajectories and fate of particles. Therefore, the injection instant alters the particle mobility with the ambient flow. In order to have a comprehensive understanding of the relation between particle behaviour and flow hydrodynamics, we used multiple injections at different times. First, the Eulerian model starts running for a specific period, until the ambient flow reaches into a quasi-steady fully developed situation. Next, MP particles with the same physical characteristics are injected in a time-sequential behaviour every 10 s. The concentration of MPs in the ambient flow is quite dilute, and therefore, MP particles do not affect the ambient flow or each other as a cloud of particles [23]. In other words, it is assumed that microplastics are discrete independent passive particles with no effective collision, which is an equivalent to the one-way coupling system [10]. Therefore, each microplastic particle is considered as a free body diagram, and based on Newton's second law, the instantaneous velocity of the particle is calculated (Eq. (6)). Here we assumed drag, buoyancy, and gravity as active force components on a MP particle:

$$m_p\frac{dv_p}{dt_p} = F_D + F_G + F_B \tag{6}$$

where m_p is the particle's mass, v_p is the particle's instantaneous velocity in vertical direction, dt_p is the Lagrangian time step, and F_D, F_G, and F_B are drag, gravity, and buoyancy force components.

In the present study, we assumed all MP particles have spherical shapes, based on two supporting facts. First, drag calculation is very critical in dynamic particle-tracking studies. The drag force and terminal velocity calculation of spherical particles is well-understood based on the existing literature. However, for irregular shapes, the calculation of the drag coefficient is still a challenging open-ended question and requires further research [4, 18]. For instance, fibres are among the most abundant

reported MP shapes, especially among bed sediments [5, 20, 29, 32]. However, the settling pattern of fibres is completely random, and therefore, the same particle might have different settling velocities as it sinks [1, 18]. The second reason for using spherical MPs is the consistent abundance of these particle shapes among reported MPs at different aquatic compartments [2, 27]. Therefore, in this study, the active vertical force components are calculated based on Eqs. (7)–(9) for a spherical MP particle:

$$F_D = \frac{1}{2}\rho_f C_D A_p |v_f - v_p|(v_f - v_p) \tag{7}$$

$$F_G = \rho_p g V_p \tag{8}$$

$$F_B = -\rho_f g V_p \tag{9}$$

where A_p is the projected area, v_f is the ambient flow instantaneous velocity in the vertical direction, ρ_p is the density of the particle, V_p is the volume of the particle, and C_D is the drag coefficient calculated using the [23] method for spherules:

$$C_D = \begin{cases} \frac{24}{\mathrm{Re}_p}\left(1 + \frac{1}{6}\mathrm{Re}_p^{\frac{2}{3}}\right), & \mathrm{Re}_p \leq 1000 \\ 0.424, & \mathrm{Re}_p > 1000 \end{cases} \tag{10}$$

where Re_p is the particle Reynolds number and is calculated based on Eq. (11):

$$\mathrm{Re}_p = \frac{d_p |v_f - v_p|}{\nu} \tag{11}$$

where d_p is the particle diameter. In each iteration, after finding the instantaneous particle velocity, MP displacement in two directions is calculated using Eq. (12):

$$\frac{\mathrm{d}x_p}{\mathrm{d}t_p} = v_p \tag{12}$$

where x_p is the instantaneous particle location.

2.3 Numerical Simulation

OpenFOAM has multiple predefined solvers for both the Eulerian and Lagrangian simulations. Current simulations are based on the PimpleFoam solver, which employs the PIMPLE algorithm for pressure calculation, and is suitable for transient flow simulation. The temporal and spatial discretization schemes are set to the Upwind

and Gauss Linear, respectively. These numerical simulations are based on the explicit scheme. Therefore, the Courant number needs to be considered as the stability criterion.

$$C_o = \frac{\overline{u}_i \mathrm{d}t_E}{\mathrm{d}x} \qquad (13)$$

where $\mathrm{d}t_E$ is the Eulerian time step. In these simulations, two different time steps are considered for the Eulerian and Lagrangian sub-models. The grid size in the current simulations is always greater than the particle size. Therefore, in each time step, the particle is located inside one of the grids, and the ambient flow characteristics need to be interpolated at the location of the particle. Furthermore, Courant number is also used for the regulation of the Lagrangian time step, $\mathrm{d}t_p$, in the particle-tracking sub-model. The Lagrangian time step, $\mathrm{d}t_p$, is then defined as the time particle requires to exit the containing cell, based on the maximum particle Courant number. The Lagrangian time steps can be smaller than or equal to the Eulerian time step.

Figure 1 depicts the general geometry of the simulations. As demonstrated, d is the inlet water depth, h is the step height, and L_1 and L_2 are lengths before and after the step, respectively. Here we used a uniform flow boundary condition with an inlet velocity of U_0 at the upstream inlet boundary (A-B), zero-gradient at the outlet and the free surface boundaries (C–D and B–C, respectively), and no-slip at the lower wall boundary (A–F–E–D). In order to minimize the effect of numerical instabilities, MP particles are injected into the ambient flow when the turbulent flow is fully developed and reaches the quasi-steady state, at a location which is adequately far from the boundaries. Also, boundaries are located far enough from the recirculation zone, to prevent probable numerical instabilities and errors.

The grids are structured, orthogonal, square mesh in the computational domain. In the present simulations, we considered a refinement zone, with a grid size of $\mathrm{d}x = \mathrm{d}y = 1.25$ cm (demonstrated in Fig. 1), and in other parts of the geometry, a coarser grid size of $\mathrm{d}x = \mathrm{d}y = 5$ cm is used.

The hydrodynamic and physical properties of all executed simulations are summarized in Table 1. In this study, based on the most abundant polymer types reported in different compartments of the aquatic environment, we considered three different
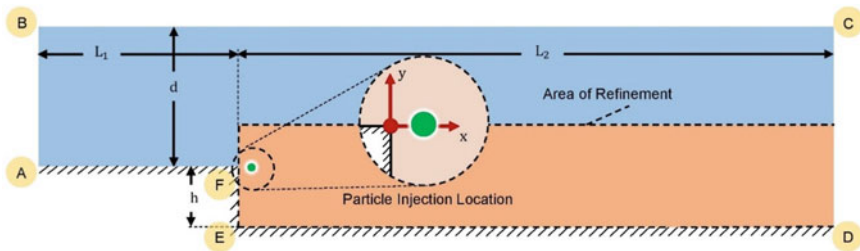
Fig. 1 Geometry of the BFS; $L_1 = 20$, $L_2 = 30$, $d = 7$, and $h = 3$ m; injection point $= (0.5, 0.0)$. The coordinate system is located at the corner of the BFS

Table 1 Executed simulations properties and IDs. These cases are simulated at three inlet velocities of 0.025, 0.100, and 0.400 m/s

Density (kg/m^3)	Size (mm)			
	0.1	0.2	0.5	2.0
PE:940	PE-S1	PE-S2	PE-S3	PE-S4
PS:1100	PS-S1	PS-S2	PS-S3	PS-S4
PET:1410	PET-S1	PET-S2	PET-S3	PET-S4

densities both for positively buoyant and negatively buoyant plastics [24]. The most abundant polymer is polyethylene (PE) with a density range of 880–970 kg/m^3, followed by polypropylene with densities ranging from 900 to 920 kg/m^3 [24]. Here, PE stands for both polyethylene and polypropylene. Also, polystyrene (PS) with densities ranging from 1040 to 1100 kg/m^3 is one of the most abundant polymer types, especially in the bed sediment. The last polymer considered in this study is polyethylene terephthalate (PET), which represents heavy particles' behaviour. Furthermore, here PET also presents the average density for polyvinyl chloride.

As discussed before, MPs have a wide range of sizes due to different weathering processes. Thus, we considered four size groups to investigate the effect of size on MPs mixing behaviour in turbulent flows. The size selection in this study is based on MPs size distribution in different compartments of the aquatic environments [24]. The size range in this study includes 2 mm, MP particles visible to the naked eye, to a smaller MP range of 200 µm. This size range is also based on the size range of sand and silt particles, which are spheroid sediment particles and a comparison target in this study. In order to investigate the role of turbulent flow in MPs vertical diffusion, we conducted multiple numerical experiments with three different inlet velocities of $U_o = 0.025$, 0.1, and 0.4 m/s. For each inlet velocity, twelve cases with different sizes and densities are simulated.

3   Results and Discussion

In turbulent flow, velocities can be decomposed into a mean value, $\overline{U}$, and a fluctuating term, u':

$$u = \overline{U} + u' \tag{14}$$

$$V = \overline{V} + v' \tag{15}$$

where u and v are the instantaneous velocity components in x- and y- directions, respectively. To determine the mean and the fluctuating components, instantaneous velocities are ensemble averaged over a period of detachment/reattachment after the quasi-steady state is achieved at $t = t_q$. Turbulent kinetic energy, k, is the parameter

Table 2 Range of mean velocity in *x*- and *y*- direction, $\overline{U}$ and $\overline{V}$, respectively, and the square root of maximum turbulent kinetic energy, $k_{\max}$, for different inlet velocities

U_0 (m/s)	$\overline{U}$ (m/s)	$\overline{V}$ (m/s)	$\sqrt{k_{\max}}$ (m/s)
0.025	[− 0.013, 0.027]	[− 0.008, 0.0104]	0.016
0.100	[− 0.048, 0.105]	[− 0.038, 0.032]	0.062
0.400	[− 0.193, 0.428]	[− 0.120, 0.158]	0.234

frequently used to quantify turbulent intensity and in a 2D flow is defined as:

$$k = \frac{1}{2}\left(\overline{u'^2} + \overline{v'^2}\right) \tag{16}$$

Table 2 summarizes the range of mean velocities, $\overline{U}$ and $\overline{V}$, and turbulent kinetic energy, k, for different ambient flow velocities of $U_o = 0.025, 0.100$, and 0.400 m/s.

The maximum and minimum velocity range of mean velocities and turbulent kinetic energy is proportional to the inlet velocity magnitude. In other words, the instantaneous characteristics of a coherent turbulent structure behind the BFS is dominated by the inlet velocity. Therefore, here we used the inlet velocity, U_o, as a representative for turbulent structure intensity. In the following sections, based on the combined characteristics of the ambient flow and MP particles, results and findings are presented in this section.

3.1 Particle Relaxation Time and the Settling Parameter

The particle relaxation time, τ_p, is defined as the time a particle needs to respond to the ambient flow changes:

$$\tau_p = \frac{\left|\rho_p - \rho_f\right| d_p^2}{18\mu} \tag{17}$$

Based on Eq. (14), particle relaxation time depends on both the particle size and the difference between the particle and ambient flow densities. This means when the particle size or its marginal density with respect to the ambient flow is relatively large compared to the ambient flow viscosity, the particle resistance to the ambient flow movements is considerable, and therefore, the particle movement needs more time to update based on flow changes. However, the particle is moving based on its natural gravitational sinking/rising behaviour in the meantime. Therefore, if the terminal velocity of the particle is considerable, the particle can skip the turbulent circulations rather than getting entrained. Figure 2 shows the effect of size and marginal density on particles entrainment with the ambient flow. As demonstrated in the picture, ambient
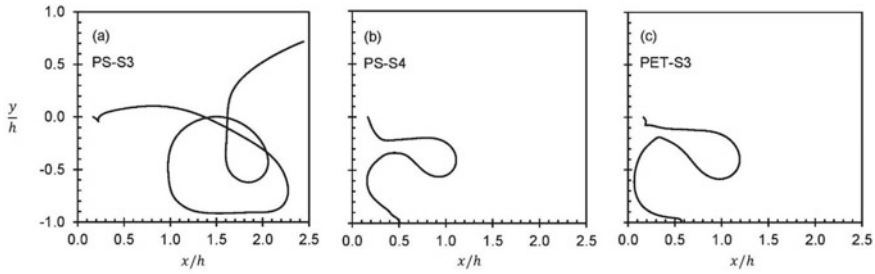
Fig. 2 Effect of particle relaxation time on MPs entrainment. The ambient flow inlet velocity, U_o, is 0.1 m/s, and all particles have the same injection time. **a** PS-S3 with diameter of 0.5 mm, **b** PS-S4 with diameter of 2.0 mm, and **c** PET-S3 with diameter of 0.5 mm. **b** and **c** demonstrate the effect of size and marginal density, respectively

flow characteristics and the injection times are the same. However, the difference in particle relaxation time due to particles characteristics results in different particle trajectories and fates. Large particles' trajectories are minimally affected by the ambient flow and are mainly governed by the particle's gravitational sinking/rising behaviour. In contrast, small relaxation time indicates the prompt particle response to ambient flow changes and therefore higher entrainment with the ambient turbulent flow.

Particle relaxation time only depends on physical properties of the particle and flow hydrodynamics. The effect of ambient flow on particle entrainment is signified by settling parameter, defined as the ratio of Stokes settling velocity, $\tau_p g$, to the ambient flow velocity scale [12, 28]. As demonstrated in Table 2, the range of mean velocity components and the turbulent kinetic energy are directly proportional to the inlet velocity, U_o. Therefore, here we used U_o as the velocity scale representative:

$$S\upsilon = \frac{\tau_p g}{\tau_f} = \frac{|\rho_p - \rho_f| g d_p^2}{18 \mu U_o} \tag{18}$$

The settling parameter determines how the particle's natural settling or rising behaviour is affected by the ambient flow movements. When the settling parameter is small, the particle tendency to its natural sinking/rising behaviour is low, and thus, the particle gets entrained with the ambient flow. On the other hand, when the settling parameter is high, the particle mainly navigates in the flow while minimally affected by the turbulent flow. Therefore, particles with high settling parameter tend to move based on their natural gravitational behaviour, which can be sinking or rising due to particle's density. Figure 3a illustrates the range of settling parameter, $S\upsilon$, for particle properties enlisted in Table 1.

In consideration for Kolmogorov microscales, dissipative time scales should be incorporated in the definition of settling parameter [23]. However, the definition of settling parameter based on Eq. (15) only incorporates the role of large-scale turbulent motions and eliminates the effect of SGS turbulent fluctuations.
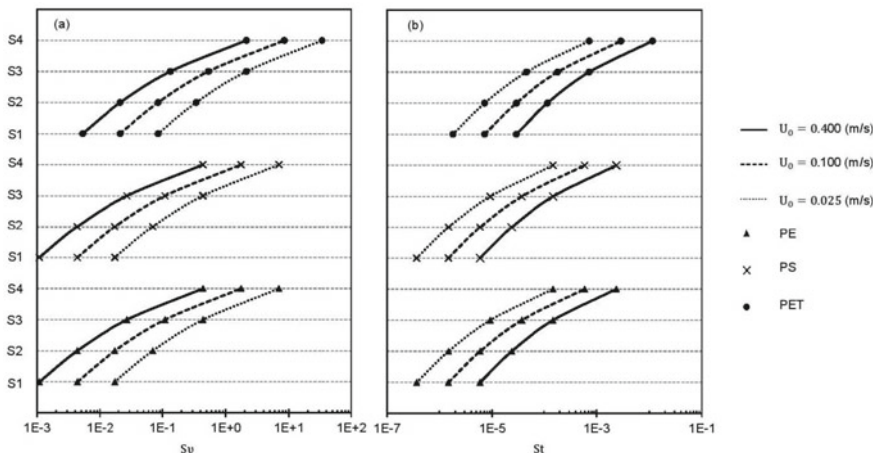
Fig. 3 **a** Range of settling parameter, $S\upsilon$, and **b** the range of stokes number, St, in the present simulations as listed in Table 1

3.2 Stokes Number and the Radius of Circulation Trapping

Another important dimensionless parameter which is commonly used in sediment analogy for particles mixing behaviour with the ambient flow is the Stokes number. Stokes number is defined as the ratio of the particle relaxation time to the flow time-scale, τ_l.

$$St = \frac{\tau_p}{\tau_l} = \frac{|\rho_p - \rho_f| d_p^2 U_0}{18 \mu h} \tag{19}$$

where τ_l is considered as the large eddy turnover time, assumed as the ratio of the step height, h, to the inlet velocity, U_o. Stokes number defines particles deviation from ambient flow parcels' movement. Therefore, when the particle is entrained with the ambient flow, Stokes number can explain whether the particle trajectory is close to the ambient flow path-lines, or it deviates from the flow. Similar to the settling parameter, Stokes number has a direct relationship with the particle size. As the size of the particle increases, the stokes number increases as well. However, in contrast with the settling parameter, Stokes number and ambient flow inlet velocity have a direct relationship, which means the Stokes number increases at higher inlet velocities. Figure 3b demonstrates the range of Stokes numbers for all executed cases. When the Stokes number is small, particle's mixing behaviour is similar to a passive tracer, and the particle follows the ambient flow path-lines closely. However, when the Stokes number is large, particle's trajectory deviates from the flow parcels' trajectories.
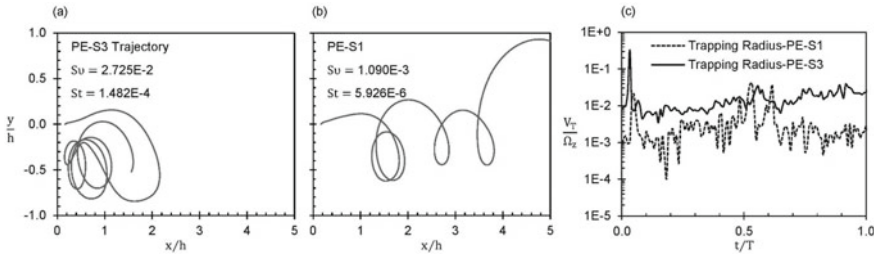
Fig. 4 Particles' trajectories, **a** and **b**, and corresponding trapping radius, **c**, at the inlet velocity of $U_o = 0.4$ m/s. As the settling parameter increase, the trapping radius increases as well. As the stokes number decreases, particle trajectory gets closer to the ambient flow path-lines

The radius of trapping explains how the particle motion deviates from the ambient flow movements. Here we used the ratio of terminal velocity to the vorticity magnitude, V_T/Ω_z, as the trapping radius [7]. When the trapping radius is small, the particle follows the flow path-lines very closely. However, when the trapping radius is high, even in a strong turbulent structure, the particle deviates from the ambient flow path-line. The trapping radius determines the circular deviation from fluid parcels. Figure 4 shows the effect of size on the radius of trapping. As the settling parameter increase, particles' resistance to turbulent diffusion intensifies. Although both trajectories in Fig. 5a and b are demonstrating fully entrained case, but only large circulations with high vorticity magnitude are capable of transporting particles with high settling parameters. As a result, as the settling parameter increases, the trapping radius increases as well. Stokes number also represents the distribution of the entrained MP particles in a turbulent flow. As demonstrated in Fig. 4, the particle with a lower stokes number is transported with the ambient flow to farther downstream locations, while the particle with a larger stokes number keeps circulating behind the step. Therefore, the Stokes number can explain the deviation of particle trajectory from flow path-lines and therefore its transport with the ambient flow.

3.3 Numerical Verification and Convergence Studies

In order to verify the results of this study, we conducted convergence experiments in computational hydrodynamic simulation to estimate the error and accuracy [16]. For this purpose, one of the fully entrained simulations, here the PE-S1 case at the inlet velocity of 0.1, is selected as the pilot simulation for convergence test. The pilot simulation is executed at three grid sizes with a refinement ratio of $r = 2$. Next, the instantaneous position of the first thirty injected particles during a full period of detachment after each particle's injection is recorded per second. In the next step, the normalized vertical position of particles, measured from the bottom of the channel at $y/h = -1$, is used to evaluate the convergence of errors and instabilities. Then
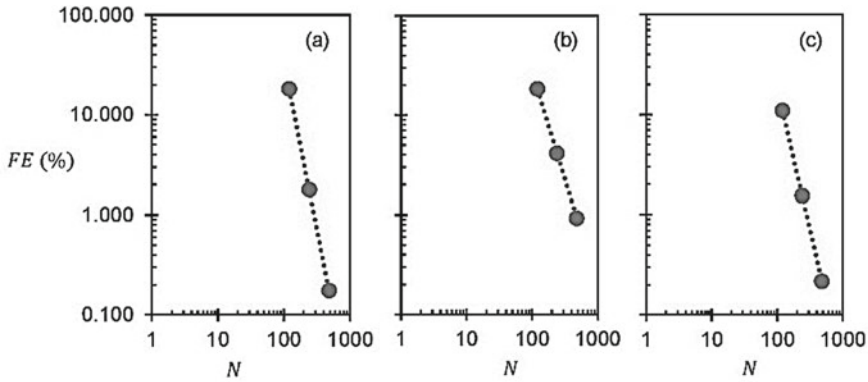
Fig. 5 Fractional computational error, FE, convergence for three grid sizes; **a**, **b**, and **c** correspond to 85, 90, and 95 percentiles, respectively

85, 90, and 95 percentiles (PR) are calculated for dataset of vertical locations in each of the simulations. The order of convergence, P_k, is then defined as

$$P_k = \frac{1}{\ln r} \ln\left(\frac{PR_k - PR_{k-1}}{PR_{k+1} - PR_k}\right) \tag{20}$$

where PR is the percentile rank, and the subscript demonstrates the level of refinement, as k for the original grid size, and $k-1$ and $k+1$ for the coarsened and refined cases, respectively. The anticipated real solution, $PR_{\Delta x \to 0}$, is then extrapolated, and the fractional computational error, FE, for each of the three simulations is calculated.

$$PR_{\Delta x \to 0} = \frac{r^{P_k} PR_{k+1} - PR_k}{r^{P_k} - 1} \tag{21}$$

$$FE = \frac{PR_n - PR_{\Delta x \to 0}}{PR_{\Delta x \to 0}} \times 100 \tag{22}$$

where PR_n is the corresponding percentile. Table 3 reports the properties as well as the convergence parameters for each of the three cases.

The fractional computational error versus the grid refinement is demonstrated in Fig. 5. The horizontal axis, N, represents the number of grids along the step height, h. The slope of the errors trendline is aligned with our spatial interpolation scheme (Gauss linear interpolation) order of error, which is two.

Table 3 Percentiles, fractional error, and order of convergence after two levels of refinement

Percentile (%)	Corresponding y- position (m)	Δx (m)	P_k	$PR_{\Delta x \to 0}$	FE (%)	N
85	1.286	2.500	3.345	1.088	18.188	120
	1.107	1.250			1.790	240
	1.090	0.625			0.176	480
90	1.384	2.500	2.154	1.169	18.382	120
	1.217	1.250			4.131	240
	1.180	0.625			0.928	480
95	1.510	2.500	2.829	1.360	11.019	120
	1.381	1.250			1.551	240
	1.363	0.625			0.218	480

4 Conclusion

The distribution and fate of aquatic MPs depend on the physical characteristics of the particle and the fluid as well as ambient flow hydrodynamics. Turbulent coherent structure plays a significant role in MPs distribution and entrainment with the flow. In this study, we conducted thirty-six numerical experiments to study the combined effect of particle properties, size and density, and turbulent intensity. We used three well-established parameters in sediment analogy to investigate MPs entrainment and distribution in a turbulent flow. The first criterion is the settling parameter which determines the tendency of a particle to its potential natural vertical settling or rising behaviour. Our results demonstrate an inverse relationship between the settling parameter and particle entrainment with the ambient flow. When the settling parameter is high, the particle tends to move based on its natural gravitational behaviour. As the settling parameter increases, particles get more entrained with the ambient flow. The second criterion is the Stokes number, which explains the distribution of particles in the turbulent flow. When the Stokes number is low, the particle's behaviour is similar to a passive tracer. However, when the Stokes number is large, the particle deviates from the ambient flow. The third criterion is the trapping radius, which similar to the Stokes number, demonstrates the circular particle diffusion around the potential position dictated by the flow. When the trapping radius is small, the particle deviation from the ambient flow is negligible, and particles closely follow the same trajectories as the fluid parcels. Therefore, in a constant flow structure, when the trapping radius is high, the particle's vertical diffusion is more considerable. However, the role of Stokes number and the trapping radius only emerge in fully entrained cases. Figure 6 shows the settling parameter versus the Stokes number for executed cases in the present simulation. When the settling parameter is high, particles are not entrained, and therefore, the Stokes number and trapping radius are not applicable. When both the settling parameter and the Stokes number are low, particles move close to flow parcels. Thus, particles are distributed to farther downstream locations
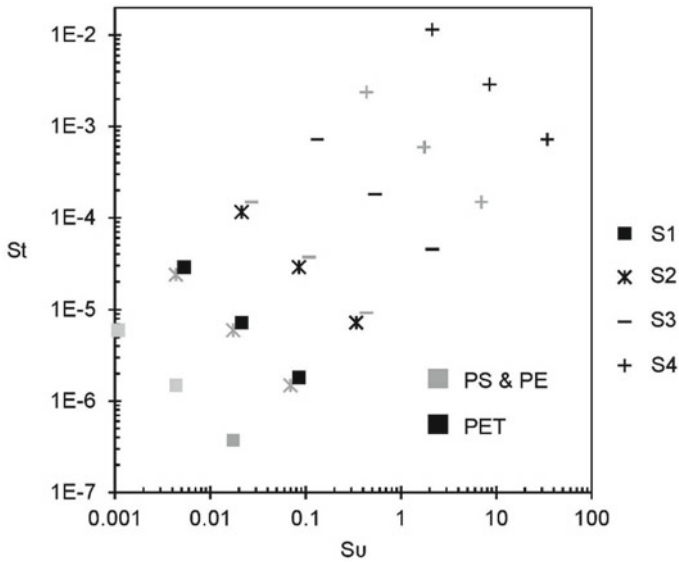
Fig. 6 Stokes number versus settling parameter for executed cases. PS and PE particles of similar size possess similar relaxation times and therefore have similar stokes numbers and settling parameters. Settling parameter determines the entrainment of the particles, while the stokes number explains the distribution of particles in the ambient flow

behind the step. In contrast, when the Stokes number is high, particles are stuck in circulations close to the step. Therefore, although particles are still fully entrained with the turbulent flow, they are concentrated in regions close to the source of injection. Further investigation is required to explain MP behaviours using combined Stokes number and settling parameter.

References

1. Bagaev A, Mizyuk A, Khatmullina L, Isachenko I, Chubarenko I (2017) Anthropogenic fibres in the Baltic Sea water column: field data, laboratory and numerical testing of their motion. Sci Total Environ 599:560–571
2. Ballent A, Corcoran PL, Madden O, Helm PA, Longstaffe FJ (2016) Sources and sinks of microplastics in Canadian Lake Ontario nearshore, tributary and beach sediments. Mar Pollut Bull 110(1):383–395
3. Barnes DK, Galgani F, Thompson RC, Barlaz M (2009) Accumulation and fragmentation of plastic debris in global environments. Philos Trans Royal Soc B: Biol Sci 364(1526):1985–1998
4. Chubarenko I, Bagaev A, Zobkov M, Esiukova E (2016) On some physical and dynamical properties of microplastic particles in marine environment. Mar Pollut Bull 108(1–2):105–112
5. Courtene-Jones W, Quinn B, Ewins C, Gary SF, Narayanaswamy BE (2020) Microplastic accumulation in deep-sea sediments from the rockall trough. Mar Pollut Bull 154:111092

6. Cózar A, Echevarria F, González-Gordillo JI, Irigoien X, Úbeda B, Hernández-León S, Palma AT, Navarro S, Garcia-de-Lomas J, Ruiz A, Fernandez-de-Puelles ML (2014) Plastic debris in the open ocean. Proc Natl Acad Sci 111(28):10239–10244
7. Dey S, Ali SZ, Padhi E (2019) Terminal fall velocity: the legacy of Stokes from the perspective of fluvial hydraulics. Proc Royal Soc A 475(2228):20190277
8. Dietrich WE (1982) Settling velocity of natural particles. Water Resour Res 18(6):1615–1626
9. Erni-Cassola G, Zadjelovic V, Gibson MI, Christie-Oleza JA (2019) Distribution of plastic polymer types in the marine environment; a meta-analysis. J Hazard Mater 369:691–698
10. Elghobashi S (1994) On predicting particle-laden turbulent flows. Appl Sci Res 52(4):309–329
11. Fornari W, Picano F, Sardina G, Brandt L (2016) Reduced particle settling speed in turbulence. J Fluid Mech 808:153–167
12. Good GH, Ireland PJ, Bewley GP, Bodenschatz E, Collins LR, Warhaft Z (2014) Settling regimes of inertial particles in isotropic turbulence. J Fluid Mech 759
13. Jalón-Rojas I, Wang XH, Fredj E (2019) A 3D numerical model to track marine plastic debris (TrackMPD): Sensitivity of microplastic trajectories and fates to particle dynamical properties and physical processes. Mar Pollut Bull 141:256–272
14. Jambeck JR, Geyer R, Wilcox C, Siegler TR, Perryman M, Andrady A, Narayan R, Law KL (2015) Plastic waste inputs from land into the ocean. Science 347(6223):768–771
15. Kane IA, Clare MA (2019) Dispersion, accumulation, and the ultimate fate of microplastics in deep-marine environments: a review and future directions. Front Earth Sci 7. https://doi.org/10.3389/feart.2019.00080
16. Ghannadi SK, Chu VH (2015) High-order interpolation schemes for shear instability simulations. Int J Num Methods Heat Fluid Flow
17. Kane IA, Clare MA, Miramontes E, Wogelius R, Rothwell JJ, Garreau P, Pohl F (2020) Seafloor microplastic hotspots controlled by deep-sea circulation. Science 368(6495):1140–1145
18. Khatmullina L, Isachenko I (2017) Settling velocity of microplastic particles of regular shapes. Mar Pollut Bull 114(2):871–880
19. Kooi M, Nes EHV, Scheffer M, Koelmans AA (2017) Ups and downs in the ocean: effects of biofouling on vertical transport of microplastics. Environ Sci Technol 51(14):7963–7971
20. Mu J, Qu L, Jin F, Zhang S, Fang C, Ma X, Zhang W, Huo C, Cong Y, Wang J (2019) Abundance and distribution of microplastics in the surface sediments from the northern Bering and Chukchi Seas. Environ Poll 245:122–130
21. Putnam A (1961) Integratable form of droplet drag coefficient. Ars J 31(10):1467–1468
22. Reisser J, Slat B, Noble K, Du Plessis K, Epp M, Proietti M, Pattiaratchi C (2015) The vertical distribution of buoyant plastics at sea: an observational study in the North Atlantic Gyre. Biogeosciences 12(4):1249–1256
23. Shamskhany A, Karimpour S (2021) The role of microplastic characteristics on vertical transport and mixing. In: Canadian society of civil engineering annual conference
24. Shamskhany A, Li Z, Patel P, Karimpour S (2021) Evidence of microplastic size impact on mobility and transport in the marine environment: a review and synthesis of recent research. Front Marine Sci 8
25. Schwarz AE, Ligthart TN, Boukris E, van Harmelen T (2019) Sources, transport, and accumulation of different types of plastic litter in aquatic environments: a review study. Mar Pollut Bull 143(March):92–100. https://doi.org/10.1016/j.marpolbul.2019.04.029
26. Smagorinsky J (1963) General circulation experiments with the primitive equations: I. Basic Exper Monthly Weather Rev 91(3):99–164
27. Song YK, Hong SH, Jang M, Kang JH, Kwon OY, Han GM, Shim WJ (2014) Large accumulation of micro-sized synthetic polymer particles in the sea surface microlayer. Environ Sci Technol 48(16):9014–9021
28. Stout JE, Arya SP, Genikhovich EL (1995) The effect of nonlinear drag on the motion and settling velocity of heavy particles. J Atmos Sci 52(22):3836–3848
29. Tekman MB, Wekerle C, Lorenz C, Primpke S, Hasemann C, Gerdts G, Bergmann M (2020) Tying up loose ends of microplastic pollution in the Arctic: distribution from the sea surface through the water column to deep-sea sediments at the HAUSGARTEN observatory. Environ Sci Technol 54(7):4079–4090

30. Terfous A, Hazzab A, Ghenaim A (2013) Predicting the drag coefficient and settling velocity of spherical particles. Powder Technol 239:12–20
31. Wang Z, Dou M, Ren P, Sun B, Jia R, Zhou Y (2021) Settling velocity of irregularly shaped microplastics under steady and dynamic flow conditions. Environ Sci Pollut Res 28(44):62116–62132
32. Zhang D, Liu X, Huang W, Li J, Wang C, Zhang D, Zhang C (2020) Microplastic pollution in deep-sea sediments and organisms of the Western Pacific Ocean. Environ Pollut 259:113948